Accepted to J. Chem. Phys. 10.1063/5.0114349

Resonant cold scattering of highly vibrationally excited D_2 with Ne

William E. Perreault, Haowen Zhou, Nandini Mukherjee*, and Richard N. Zare*

Department of Chemistry, Stanford University, Stanford, CA 94305, USA

*Corresponding authors. Emails: nmukherj@stanford.edu, zare@stanford.edu

Abstract

To accurately map weak D_2-Ne long-range interactions, we have studied rotationally inelastic cold scattering of D_2 prepared in the vibrationally excited (v=4) and rotationally aligned (j=2,m) quantum state within the moving frame of a supersonically expanded mixed molecular beam. In contrast to earlier high energy D_2-Ne collision experiments, the (j=2→j'=0) cold scattering produced highly symmetric angular distributions that strongly suggest a resonant quasi-bound collision complex that lives long enough to make a few rotations. Our partial wave analysis indicates that the scattering dynamics is dominated by a single resonant l=2 orbital, even in the presence of a broad temperature (0-5K) distribution that allows incoming orbitals up to l=5. The dominance of a single orbital suggests that the resonant complex stabilizes through the coupling of the internal (j=2) and orbital (l=2) angular momentum to produce a total angular momentum of J=0 for the D_2-Ne complex.

Long-range molecular forces play an important role in a diverse array of physical processes ranging from initiating chemical reactions to cooling the interstellar medium. However, these weak long-range interactions are poorly interrogated both by spectroscopy and high-energy molecular collisions. Only low-energy (cold) scattering experiments with molecules prepared in precisely defined quantum states, where the effects of these weak forces are manifested in various quantum effects such as tunneling resonances, are sensitive enough to precisely measure them.[1–4] This is demonstrated by the substantial progress that recent research efforts on the study of cold and ultracold collisions have made on our understanding of molecular forces at the most fundamental quantum level.[5–21] Further understanding of these quantum interactions relies on our ability to increase the direct correspondence between experimental measurements and theoretical calculations. This can only be achieved by completely controlling a theoretically tractable scattering system, for example, by examining the scattering of a molecule like H_2 prepared in a precisely defined quantum state.[22–25] To accurately map long-range interactions, the relative alignment of the colliding species or the collision geometry must also be controlled because low-temperature collisions are highly sensitive to the anisotropic molecular forces.[20,26,27]

Although rotationally inelastic scattering of H_2 with rare gas atoms is an attractive computational target owing to its theoretical tractability, experimental studies on these systems remain rare. In the past, only a few experiments at collision temperatures of ~1000 K had been performed on these fundamental systems.[28–31] Due to their high collision energies, these experiments failed to produce sufficiently accurate data on the weak long-range interactions for comparison with theory. Moreover, in these experiments, neither the initial states nor the molecular alignments were defined, further limiting their interpretation. Recently, we studied rotationally inelastic cold scattering using vibrationally excited (v = 1, 2) and rotationally aligned (j = 2, m) HD and D_2 molecules against He in a supersonically expanded mixed molecular beam.[32–34] Here, v and j represent the quantum numbers of the vibrational and rotational energy levels and m refers to the projection of the rotational angular momentum $\boldsymbol{j}$ onto a suitable quantization axis. These experiments repeatedly showed that the measured angular distribution depends sensitively on the initial quantum state and alignment of the molecular bond axis, reflecting the anisotropic nature of the long-range interaction. Additionally, these experiments demonstrated that characteristics of the dynamic resonances are fingerprinted in the features of the angular distribution that is generated by the interference of a few outgoing partial waves relating to a single resonant incoming orbital.[33] Although the Δj =2 rotational excitation of D_2 by collision with Ne has been extensively studied at high collision energies,[29] there has been no previous work on D_2-Ne scattering at low collision energies. As such, our understanding of the long-range portion of the interaction potential of this fundamental system has been highly limited.

In this work, we have carried out rotationally inelastic cold scattering experiments on D_2 with Ne to accurately map out the long-range interactions in this system. As opposed to our previous scattering experiment of D_2 with He, the D_2-Ne scattering in a molecular beam provides a unidirectional collision velocity distribution that clearly breaks symmetry between the forward and backward scattering. To experimentally measure the quantum state controlled rotational relaxation at a temperature of a few degrees Kelvin, we needed to prepare the D_2 molecule in a vibrationally excited (v = 4) and rotationally aligned (j = 2, m) quantum state. To our knowledge, this is the first experimental study of low temperature collision of D_2 molecules in highly vibrationally excited like (v = 4) where the molecule can no longer be treated as a rigid rotor. In this highly vibrationally excited state, the D_2 bond length is considerably more likely to be n near the outer classical turning point of its anharmonic potential, which will modify the D_2 (v = 4) + Ne

interaction potential energy surface (PES) from the one determined from studies of D_2 ($v = 0$) + Ne scattering. Indeed, we were unable to measure any scattering of the ($v = 0$) ground state or the ($v = 2$) vibrationally excited state of the D_2 molecules at the low temperatures present in our experiment. In contrast to all of the previous high energy D_2-Ne rotational excitation scattering experiments that showed backward scattering,[29,30] our experiment studying the ($j = 2 \rightarrow j' = 0$) rotational relaxation shows a scattering angular distribution that is not only highly symmetric with respect to the forward and backward directions, but has higher depth of modulation compared to our previous scattering between D_2 and He. The observed symmetry of the angular distribution strongly supports the presence of a scattering resonance that has a sufficiently long lifetime to support at least one rotation of the collision complex.[6,14,35] Probing further into the nature of the quasi-bound D_2-Ne complex using partial wave analysis indicates that the resonant state has a preference for a particular total angular momentum state.

The $\Delta j = 2$ rotational relaxation of D_2 ($v = 4$, $j = 2$) via collision with atomic Ne is studied in a supersonically expanded and collimated mixed molecular beam (D_2:Ne = 1:5). The highly collimated molecular beam defines a direction with respect to which we align the molecular axis. Figure 1a shows a large velocity slip between the lab frame velocity distributions of D_2 and Ne in the mixed molecular beam. These distributions were measured by separately ionizing each of the two species in the REMPI probe volume within the molecular beam and fitting their measured time-of-flight distributions as described in the supplement and detailed in our earlier publications.[36,37] The Ne was ionized using (3+1) resonance enhanced multiphoton ionization (REMPI) using UV laser pulses at 220.768 nm to match the three photon resonance with the $2s^2 2p^5(^2P^\circ_{1/2})3s$ state, determined earlier by Saloman and Sansonetti.[38] As we have observed in our earlier experiments,[37] the co-expansion of a lighter with a heavier gas in a supersonic beam accelerates the heavier species such that it moves faster than the lighter species, although the real reason of this behavior is not clearly understood. Figure 1b shows the nearly unidirectional relative velocity (collision velocity), which is calculated by convoluting the lab frame velocities of the two colliding partners. The co-expansion in a single molecular beam reduces the magnitude of the relative velocity producing a corresponding collision temperature of a few degrees Kelvin in the moving frame of the mixed molecular beam. In our earlier work, the collision velocity distribution in the moving frame of the mixed molecular beam was nearly symmetric about zero velocity because the partner molecules had similar masses (D_2-He, D_2-HD, HD-H_2). A symmetric collision velocity distribution will always generate a measured scattering angular distribution that is symmetric about 90° irrespective of the symmetry of the differential cross section for the scattering process. On the other hand, the large velocity slip present here for the D_2-Ne mixed beam breaks this symmetry, making it possible to directly measure any asymmetry of the differential cross section that may be present.

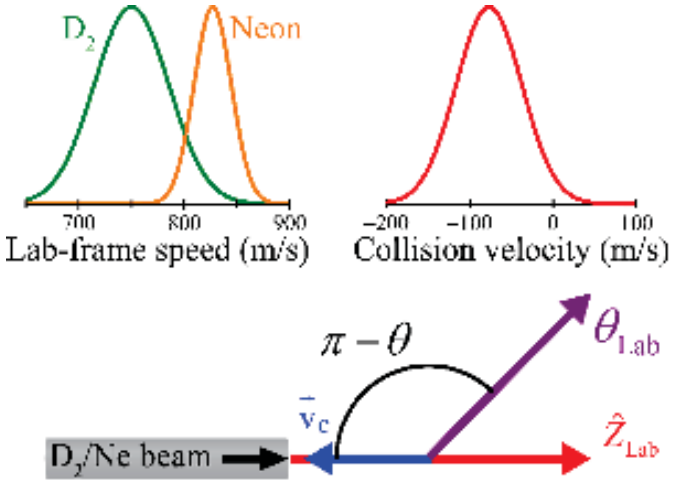

Figure 1. Measured D_2-Ne collision velocity distribution in a single co-expanded molecular beam. (a) Lab-frame velocity distributions of the D_2 and Ne molecules at the probe site. These distributions were determined by fitting the measured time-of-flight distributions of each of the two species in the beam. (b) Collision velocity distribution in the moving frame of the molecular beam. Because of the large velocity slip between D_2 and Ne, the collision velocity is highly asymmetric, producing nearly unidirectional collisions where the D_2 velocity is oriented antiparallel to the molecular beam. (c) Diagram relating the D_2-Ne center-of-mass scattering angle θ with the lab-frame angle θ_{Lab}. Because the collision velocity v_c is negative with respect to the lab-frame axis Z_{Lab}, the measured scattering rate at the lab-frame angle θ_{Lab} becomes the scattering angle π-θ in the center-of-mass frame.

For a given collision velocity distribution $f(v_c)$, the differential scattering rate can be written as

$$I(\theta_{Lab}=\theta)=\int_0^{+\infty}\sigma(\theta)|v_c|f(v_c)dv_c+\int_{-\infty}^{0}\sigma(\pi-\theta)|v_c|f(v_c)dv_c \quad (1)$$

taking both positive and negative collision velocity groups into account. In Eq. (1), the scattering angle θ is defined in the center-of-mass frame. The experimentally measured scattering rate at the lab-frame angle θ_{Lab} with respect to the molecular beam axis Z_{Lab} is thus generated from forward scattering ($\theta_{Lab}=\theta$) of the positive collision velocity group, and backward scattering ($\theta_{Lab}=\pi-\theta$) of the negative group. For a symmetric velocity distribution, $f(v_c)=f(-v_c)$, Eq. (1) generates a differential scattering rate $I(\theta_{Lab})$ that is fully symmetric about $\theta_{Lab}=\pi/2$ irrespective of the symmetry of the scattering cross-section $\sigma(\theta)$

$$I(\theta_{Lab}=\theta)=\int_0^{+\infty}\left[\sigma(\theta)+\sigma(\pi-\theta)\right]|v_c|f(v_c)dv_c \quad (2)$$

On the other hand, for the highly asymmetric, nearly unidirectional D_2-Ne collision velocity distribution shown in Figure 1, we can neglect the contribution of the positive collision velocity group, reducing Eq. (1) to

$$I(\theta_{Lab}=\theta)\cong\int_{-\infty}^{0}\sigma(\pi-\theta)|v_c|f(v_c)dv_c, \quad (3)$$

where only the negative collision velocity group is present. Eq. (3) demonstrates that measured symmetry in the scattering angular distribution of collisions with a nearly unidirectional collision velocity reflects a fundamentally symmetric character of the differential scattering cross-section, which is associated with a scattering resonance. Thus, the highly symmetric angular distribution measured for the $\Delta j = 2$ rotationally inelastic D_2-Ne scattering strongly suggests a resonant quasi-bound state for the D_2-Ne collision complex.

To prepare a large, scattering-sensitive population of vibrationally excited and rotationally aligned D_2 ($v = 4$, $j = 2$) molecules, we have used the two-step Stark induced adiabatic Raman passage (double SARP)[39] that we have recently demonstrated.[40] As described at length in our earlier publication,[40] double SARP combines a nanonsecond Stokes pulse at 1064 nm with two delayed nanosecond pump pulses at 648 nm and 676 nm to produce D_2 ($v = 4$, $j = 2$). Two specific D_2 bond axis alignments (HSARP and XSARP) are prepared by combining specific polarization directions of the pump and Stokes laser pulses[41] using a fast switching Pockels cell. A detailed description of polarization control in double SARP is given in the supplementary material. The molecular bond axis in the HSARP ($j = 2$, $m = 0$) state is preferentially aligned along the collision velocity direction, which lies parallel to the lab-frame molecular beam axis that we choose for the quantization Z axis as shown in Fig. 1c. In the XSARP $1/\sqrt{2}$ [($j = 2$, $m = 1$) + ($j = 2$, $m = -1$)] state, the two coherently coupled bond axes are preferentially aligned at 45 degrees relative to the quantization Z axis. For each case we measure the scattered product D_2 ($v = 4$, $j' = 0$) state selectively using (2+1) resonance enhanced multi-photon ionization (REMPI). The measured scattering angular distributions for the two bond axis alignments are displayed in Fig. 2.

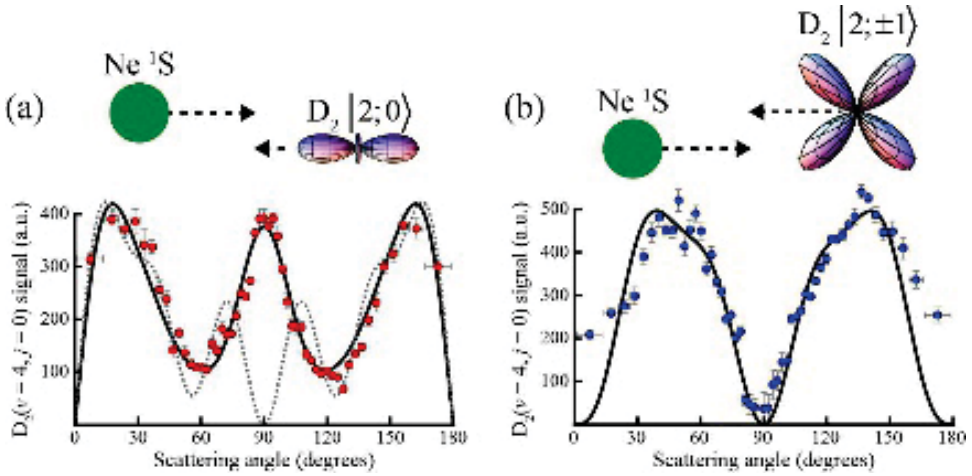

Figure 2. Collision geometries and measured angular distributions for D_2-Ne scattering for (a) HSARP and (b) XSARP. The solid curves in the HSARP and XSARP plots give the fits of the scattering angular distributions using only even ($l' = 0, 2, 4, 6$) outgoing orbitals. The dashed curve in the HSARP plot gives the fit using only odd ($l' = 1, 3, 5, 7$) outgoing orbitals. Clearly, the odd outgoing orbitals fail to fit the experimental data, whereas even outgoing orbitals produce a fit that accurately reproduces our measurements. The fits using the even orbitals have R^2 values of 0.98 and 0.97 for HSARP and XSARP, respectively.

To understand more deeply the highly symmetric angular distribution, we use a partial wave analysis that is based on the conservation of total angular momentum and symmetry during the $\Delta j = 2$ quadrupolar transition. A detailed description of the partial wave analysis is given in the supplementary material and our earlier publications.[32,33] Briefly, the scattering angular distribution for a coherently prepared input quantum state $\sum_m a_m |j,m\rangle$ can be expressed as

$$\frac{\mathrm{d}\sigma}{\mathrm{d}\theta} = \sin\theta \int_0^{2\pi} \left| \sum_m a_m \, q_{j=2,m\to j'=0} \right|^2 \mathrm{d}\varphi, \tag{4}$$

where a_m gives the amplitude of the m states and $q_{j=2,m\to j'=0}$ represents the probability amplitude to find the scattered D_2 ($v = 2, j' = 0$) from the initial state $|j=2,m\rangle$ within a differential solid angle $d\Omega$ in a direction defined by the polar angle θ and azimuthal angle φ. The scattering amplitude $q_{j=2,m\to j'=0}$ can be expressed as the coherent superposition of the outgoing orbitals

$$q_{j=2,m\to j'=0} = \sum_{l',m_{l'}} c_{l'm_{l'}} \mathrm{Y}_{l'm_{l'}}(\theta,\varphi), \tag{5}$$

where the complex expansion coefficient $c_{l'm_{l'}}$ gives the corresponding amplitude of the outgoing orbital with angular momentum l' and its projection onto the quantization z axis $m_{l'}$ represented by the spherical harmonic $\mathrm{Y}_{l'm_{l'}}(\theta,\varphi)$. The contribution of each outgoing orbital can be determined by fitting the experimental angular distributions using Eqs. (4) and (5). Note that each outgoing orbital results from the scattering of the coherently coupled incoming orbital states l. Therefore, partial wave analysis allows us to extract information on the dynamics of the rotationally inelastic collision. In the presence of a scattering resonance, a single incoming orbital dominates, generating a small number of outgoing orbitals that produce characteristic features in the angular distribution.

To determine the possible scattered orbitals l', we must first determine the incoming orbitals that may contribute to the scattering process. As shown in Figure 3, we consider the adiabatic potential[29] for each individual partial wave l as described in the figure caption and the collision rate factor for the range of temperatures present in our experiment. The collision rate factor $g(\mathrm{T})$ is defined as $g(\mathrm{T}) = \mathrm{v}_c(\mathrm{T}) \times f_c(\mathrm{v}_c(\mathrm{T}))$, where $\mathrm{v}_c(\mathrm{T})$ is the D_2-Ne collision speed and $f_c(\mathrm{v}_c(\mathrm{T}))$ gives the probability to find this collision speed, determined from the collision velocity distribution in Fig. 1b. Figure 3 shows the incoming orbitals that fall within the available range of our collision temperature and can therefore contribute to our measured distribution are $l = 2, 3, 4, 5$. Following the selection rule $\Delta l = 0, \pm 2$ for quadrupolar transitions, these incoming orbitals can generate the outgoing orbitals $l' = 0, 1, 2, 3, 4, 5, 6, 7$. We determine the relative significance of the scattered orbitals by partial wave analysis as well as symmetry considerations.

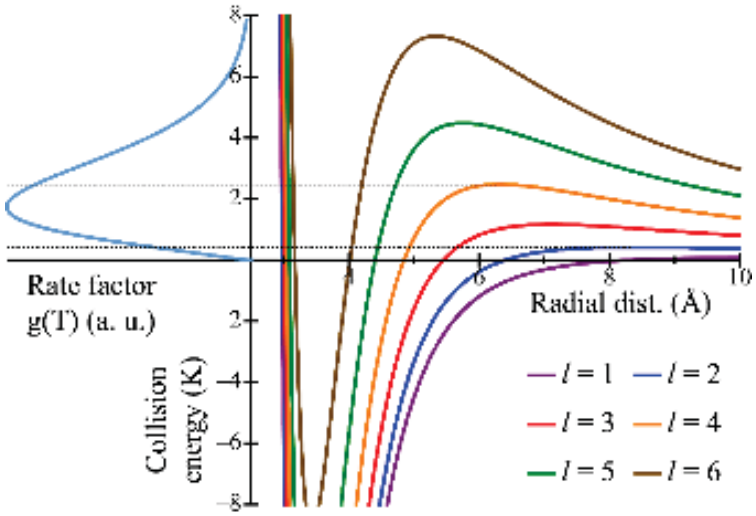

Figure 3. D_2-Ne adiabatic potentials for the incoming partial waves l = 1-6 (right) and the collision rate factor as a function of collision energy (left). The vertical axis is shared to enable easy comparison. The effective potentials $V_{eff}(R,l)$ are calculated using the equation $V_{eff}(R,l) = V(R) + \frac{l(l+1)\hbar^2}{2\mu R^2}$, where $V(R)$ is the rigid rotor potential determined by Andres et al. [29] using the D_2 (v = 0) equilibrium bond length and setting the angle between the bond axis and the radial vector $\boldsymbol{R}$ connecting the D_2 and Ne centers-of-mass θ = 0, and μ is the reduced mass. The collision rate factor g(T) is defined as $g(\mathrm{T}) = \mathrm{v}_c(\mathrm{T}) \times f_c(\mathrm{v}_c(\mathrm{T}))$. The two dashed lines have been drawn to compare the rate factors at the peaks of the centrifugal barriers for l = 2 and l = 4, which the partial wave analysis described below identifies as the prominent incoming partial waves contributing to this scattering process.

The partial wave analysis is most straightforward and reliable in the HSARP case, where a single incoming state is scattered into a single outgoing state, and so we analyze it first to determine the relative contributions of the outgoing orbitals. We then confirm these outgoing orbitals by checking their ability to fit the XSARP distribution. From the conservation the Z component of the total angular momentum, the partial waves contributing to the HSARP scattering are represented by the spherical harmonics $Y_{l'0}(\theta, \varphi)$ that have well-defined parity given by $(-1)^{l'}$. As a consequence, the highly symmetric HSARP angular distribution must be composed of outgoing partial waves that have identical parity, meaning that they are either all even or odd. In Figure 2a, the dashed curve shows the fit to the D_2-Ne HSARP scattering angular distribution produced using only the odd outgoing orbitals l' = 1, 3, 5, 7, while the solid black curve shows the fit produced using exclusively the even orbitals l' = 0, 2, 4, 6. Clearly the fit using the odd orbitals fails to reproduce the angular distribution, while the interference of the even outgoing orbitals generates a good fit for the measured distribution giving a R^2 = 0.98. Likewise, the even outgoing orbitals also produce a good fit to the XSARP scattering as shown

by the solid black curve in Fig. 2b. Following the selection rule for quadrupolar interactions, these even orbitals can only arise from the scattering of the even incoming orbitals, $l = 2$ and 4. Does this imply that both $l = 2$ and $l = 4$ contribute resonantly to the inelastic scattering, supporting two distinct quasi-bound states in their respective centrifugal wells for the D_2-Ne complex? To answer this question, we must look into the relative amplitudes of the outgoing partial waves.

Using angular momentum conservation, we find that the outgoing orbitals $l' = 0$, 2, 4 arise from the scattering of the incoming orbital $l = 2$, whereas the incoming orbital $l = 4$ gives rise to the outgoing orbitals $l' = 2$, 4, 6. The partial wave fit to the HSARP scattering generates the largest amplitude for the outgoing $l' = 0$ state, while the amplitude for the $l' = 6$ state is an order of magnitude weaker. Moreover, excluding $l' = 6$ from the set of outgoing orbitals hardly changes the R^2 of the fit, emphasizing that this orbital has the least significance in fitting the measured distribution. We note that the strongest outgoing wave $l' = 0$ arises exclusively from the scattering of the $l = 2$ orbital, whereas the substantially weaker $l' = 6$ originates only from the incoming $l = 4$ orbital. This clearly suggests the dominance of the $l = 2$ over the $l = 4$ orbital, and a likely $l = 2$ resonance for the D_2-Ne scattering. The presence of a single scattering resonance as opposed to multiple resonances is supported by the extraordinarily sharp features of the measured HSARP and XSARP angular distributions. These sharp features would be absent in the presence of multiple resonances that belong to different collision velocity groups, because the absence of phase coherence between the scattered waves originating from different resonances prevents them from interfering with one another. Additionally, we note that the characteristic features of the measured angular distribution for both HSARP and XSARP scattering are very much representative of the $l = 2$ resonant scattering theoretically predicted and measured in our earlier cold scattering experiments.[33] The sharp contrast of the XSARP scattering at 90 degrees as compared to the forward and backward directions, going all the way to zero is a characteristic feature of a pure $l = 2$ resonance according to prior theoretical calculations.[42]

The dominance of the $l = 2$ over the $l = 4$ orbital, however, seems to be contradicted by comparison of the rate factor with the adiabatic potentials plotted in Figure 3. We know that the orbiting resonance for a given partial wave should have an energy close to the peak of the centrifugal barrier for that partial wave. Clearly, the collision rate factor near the peak of the $l = 4$ potential is approximately twice as large as that near the peak of the centrifugal barrier of the $l = 2$ potential. From the coupling of the internal angular momentum $j = 2$ with the orbital angular momentum $l = 2$, we determine the possible values of the total angular momentum $J = 0$, 2, 4 for the D_2-Ne collision system. The partial wave analysis of HSARP scattering indicates that the $J = 0$ (corresponding to the $l' = 0$) scattering has the largest amplitude, which suggests that the D_2-Ne resonant complex prefers this angular momentum state. The $J = 0$ state would be inaccessible with the incoming orbital $l = 4$, which might explain the relatively weaker contribution of this orbital. Additionally, the $J = 0$ state would also be inaccessible by the $l = 3$ and the $l = 5$ orbitals, supporting their absence in the scattering angular distribution.

To further understand the significance of the quasi-bound state with total angular momentum $J = 0$ in the D_2-Ne $\Delta j = 2$ quadrupolar transition, we also examined the D_2 ($v = 4$, $j = 4$) $\rightarrow$ D_2 ($v = 4$, $j' = 2$) relaxation via collision with Ne. Although the radial portion of the scattering potential and the collision energy distribution are identical to those involved in the D_2 ($v = 4$, $j = 2$) $\rightarrow$ D_2 ($v = 4$, $j' = 0$) relaxation, we found that the experimentally measured scattering rate of D_2 ($v = 4$, $j = 4$) $\rightarrow$ D_2 ($v = 4$, $j' = 2$) is dramatically weaker, reducing by substantially more than an order of magnitude to fall below our background noise level. To a

first order approximation, the state mixing probability drops with the square of the energy difference between the initial and final state. Away from resonance, the first order perturbation to the interaction Hamiltonian gives the transition probability from the initial eigenstate $|m\rangle$ to a final eigenstate $|k\rangle$ as proportional to $|U_{mk} / E_{mk}|^2$, where U_{mk} gives the interaction energy connecting the two states, and E_{mk} gives the difference in their energies. From the ratio of the relaxation energies in the two $\Delta j = 2$ relaxations, we expect the $j = 4 \rightarrow j' = 2$ scattering rate to be reduced by only a factor of five, which is clearly insufficient to explain our observation.

We would like to emphasize that the scattering for rotational relaxation of a hydrogen molecule in its electronic ground state by an inert atom at low collision energies is generally weak to the point of being unmeasurable in the absence of resonance. This is because the atom-diatom van der Waals interaction U is an order of magnitude weaker than E_{mk} for transitions between low-lying rotational levels of the hydrogen molecules. The scattering rate for the collisions we study here will thus be very weak in the absence of a resonant quasi-bound state to enhance the cross-section. We thus believe that the suppression of $j = 4 \rightarrow j' = 2$ beyond that due to the larger relaxation energy is caused by its inability to access the resonant state. To clarify this, we carefully examine the partial cross-sections for the resonant total angular momentum $J = 0$ state for both of the $\Delta j = 2$ transitions.

Following Arthurs and Dalgarno,[43] we can write out the expression for the partial wave cross section $\sigma(J; j \rightarrow j')$

$$\sigma(J; j \rightarrow j') \propto \left| \sqrt{2l+1} \left\langle JM \middle| jm_j, lm_l \right\rangle \left\langle JM \middle| j'm_{j'}, l'm_{l'} \right\rangle \right|^2, \tag{6}$$

where $\left\langle JM \middle| jm_j, lm_l \right\rangle$ represents the Clebsch-Gordan coefficient coupling the rotational angular momentum $\left| jm_j \right\rangle$ with the orbital angular momentum $\left| lm_l \right\rangle$ to produce $\left| JM \right\rangle$. For the $j = 2 \rightarrow j' = 0$ HSARP scattering, the quasi-bound state with total angular momentum $J = 0$ is generated by coupling the rotational angular momentum $j = 2$ with the incoming orbital angular momentum $l = 2$. Angular momentum is conserved in the outgoing channel by coupling the scattered angular momentum $j' = 0$ with the outgoing orbital $l' = 0$. The partial cross-section to form the $J = 0$ bound state in $j = 2 \rightarrow j' = 0$ scattering is thus

$$\sigma(0; 2 \rightarrow 0) \propto \left| \sqrt{2l+1} \langle 00 | 20, 20 \rangle \langle 00 | 00, 00 \rangle \right|^2. \tag{7}$$

For the $j = 4 \rightarrow j' = 2$ HSARP scattering, the $J = 0$ quasi-bound state is generated by coupling the internal $j = 4$ state with the incoming orbital $l = 4$, and angular momentum is conserved by coupling the scattered $j' = 2$ state with the outgoing orbital $l' = 2$. Assuming polarization preserving (m_j-$m_{j'} = 0$) collisions, the partial cross-section to form the $J = 0$ state in $j = 4 \rightarrow j' = 2$ scattering is

$$\sigma(0; 4 \rightarrow 2) \propto \left| \sqrt{2l+1} \langle 00 | 40, 40 \rangle \langle 00 | 20, 20 \rangle \right|^2. \tag{8}$$

From Eqs. (7) and (8) we find that $\sigma(0; 2 \rightarrow 0) / \sigma(0; 4 \rightarrow 2) \approx 5$, demonstrating that the $J = 0$ quasi-bound state is less strongly coupled to the $j = 4 \rightarrow j' = 2$ transition. This additional geometric factor of five when combined with the energy factor explains the small cross section for the $j = 4 \rightarrow j' = 2$ transition we have measured and further supports the $J = 0$ quasi-bound state in these D_2-Ne $\Delta j = 2$ relaxation collisions.

Our ability to prepare a large quantity of D_2 molecules in a highly vibrationally excited ($v = 4$) and rotationally aligned quantum state has allowed us to observe the cold inelastic ($j = 2 \rightarrow j' = 0$) scattering of D_2 with Ne within a mixed molecular beam. As opposed to our earlier cold scattering experiments on similar light weight species, like D_2-He in a single beam, D_2-Ne offers a unique situation where the collision velocity is unidirectional, and the reduced mass is nearly twice as large. The large velocity slip of the D_2-Ne beam and the increased reduced mass generate a collision temperature distribution that extends up to 5 Kelvin allowing a larger number of incoming orbitals l =1-5 to contribute to this collision. Under this condition, we were surprised to observe a highly symmetric D_2-Ne scattering angular distribution that can be generated only when there is a single dominant resonant orbital. The observed symmetry is characteristic of a resonant state that lives long enough to support at least one full rotation of the collision complex. Pessimistically assuming a radius for the orbiting complex $R = 5$ Å,[44] we can estimate the moment of inertia $I = \mu R^2$, which gives the rotation period $T = 33$ ps for the $l = 2$ orbital of the D_2-Ne complex. We can also estimate the complex lifetime $\tau_c \sim h / \Delta E$, where ΔE is the width of the resonance. Taking the maximum possible value $\Delta E = 0.4$ K for the width of the $l = 2$ shape resonance, we estimate the complex lifetime $\tau_c = 117$ ps, which clearly supports more than three rotations of the complex as would be expected from the symmetry of the measured scattering distribution.

The measured distribution not only shows a nearly ideal $l = 2$ shape resonance structure, the existence of this resonance is also supported by our partial wave analysis. This inspires the question, why does a single resonance dominate the dynamics of the cold collision when there is a broad temperature distribution supporting a number of possible orbiting resonances? In fact, the collision rate factor shown in Fig. 3 is far greater at temperatures close to the peak of the centrifugal barriers of the $l = 3$ and $l = 4$ orbitals. The $l = 2$ shape resonance has also been observed for D_2–He cold collisions, where the temperature limited the number of contributing partial waves to only $l = 0$, 1, 2. For the D_2-Ne collisions, because a relatively larger number of the orbitals contribute to the scattering process, the dominance of the $l = 2$ wave is more surprising and arises from the fundamental nature of the $\Delta j = 2$ quadrupolar transition. Based on our analysis, it seems likely that the quasi-bound state is stabilized by coupling the rotational angular momentum ($j = 2$) and the orbital angular momentum ($l = 2$) producing a total angular momentum state $J = 0$. Thus, quantum-controlled D_2-Ne cold scattering not only generates new and important experimental data for understanding the long-range interactions in this fundamental collision process, it also opens new questions regarding the dynamic character of resonant complexes in general.

Supplementary material

See the supplementary material for a description of experimental set up used for polarization control of two-step SARP, details on the experimental determination of the collision velocity distribution, and details on the partial wave analysis.

Acknowledgements

This work was supported by the U.S. Army Research Office through the MURI program under grant no. W911NF-19-1-0283 and the National Science Foundation under grant no. PHY-2110256.

Data availability

The experimental data supporting this study are available from N.M. on request.

References

1. Weck, P. F. & Balakrishnan, N. Importance of long-range interactions in chemical reactions at cold and ultracold temperatures. *Int. Rev. Phys. Chem.* **25**, 283–311 (2006).
2. Balakrishnan, N. On the role of van der Waals interaction in chemical reactions at low temperatures. *J. Chem. Phys.* **121**, 5563–5566 (2004).
3. Costes, M. & Naulin, C. Observation of quantum dynamical resonances in near cold inelastic collisions of astrophysical molecules. *Chem. Sci.* **7**, 2462–2469 (2016).
4. Naulin, C. & Costes, M. Experimental search for scattering resonances in near cold molecular collisions. *Int. Rev. Phys. Chem.* **33**, 427–446 (2014).
5. Shagam, Y. & Narevicius, E. Sub-Kelvin collision temperatures in merged neutral beams by correlation in phase-space. *J. Phys. Chem. C* **117**, 22454–22461 (2013).
6. Paliwal, P., Deb, N., Reich, D. M., Avoird, A. van der, Koch, C. P. & Narevicius, E. Determining the nature of quantum resonances by probing elastic and reactive scattering in cold collisions. *Nat. Chem.* **13**, 94–98 (2021).
7. Balakrishnan, N. & Dalgarno, A. Chemistry at ultracold temperatures. *Chem. Phys. Lett.* **341**, 652–656 (2001).
8. Morita, M. & Balakrishnan, N. Stereodynamics of rotationally inelastic scattering in cold He + HD collisions. *J. Chem. Phys.* **153**, 091101 (2020).
9. Balakrishnan, N., Forrey, R. . & Dalgarno, a. Threshold phenomena in ultracold atom–molecule collisions. *Chem. Phys. Lett.* **280**, 1–4 (1997).
10. Carr, L. D., DeMille, D., Krems, R. V. & Ye, J. Cold and ultracold molecules: Science, technology and applications. *New J. Phys.* **11**, (2009).
11. Ospelkaus, S., Ni, K. K., Wang, D., de Miranda, M. H. G., Neyenhuis, B., Quéméner, G., Julienne, P. S., Bohn, J. L., Jin, D. S. & Ye, J. Quantum-State Controlled Chemical Reactions of Ultracold Potassium-Rubidium Molecules. *Science* **327**, 853–857 (2010).
12. Stuhl, B. K., Hummon, M. T. & Ye, J. Cold State-Selected Molecular Collisions and Reactions. *Annu. Rev. Phys. Chem.* **65**, 501–518 (2014).
13. Jankunas, J. & Osterwalder, A. Cold and Controlled Molecular Beams: Production and Applications. *Annu. Rev. Phys. Chem.* **66**, 241–262 (2015).
14. de Jongh, T., Besemer, M., Shuai, Q., Karman, T., van der Avoird, A., Groenenboom, G. C. & van de Meerakker, S. Y. T. Imaging the onset of the resonance regime in low-energy NO-He collisions. *Science* **368**, 626–630 (2020).
15. Chefdeville, S., Kalugina, Y., van de Meerakker, S. Y. T., Naulin, C., Lique, F. & Costes, M. Observation of Partial Wave Resonances in Low-Energy O_2-H_2 Inelastic Collisions. *Science* **341**, 1094–1096 (2013).
16. Brouard, M., Chadwick, H., Gordon, S. D. S., Hornung, B., Nichols, B., Kłos, J., Aoiz, F. J. & Stolte, S. Fully quantum state-resolved inelastic scattering of NO(X) + Kr: Differential cross sections and product rotational alignment. *J. Chem. Phys.* **141**, 164306 (2014).
17. Wang, F., Lin, J.-S. & Liu, K. Steric Control of the Reaction of CH Stretch – Excited CHD_3 with Chlorine Atom. *Science* **331**, 900–904 (2011).
18. Vogels, S. N., Onvlee, J., Chefdeville, S., Van Der Avoird, A., Groenenboom, G. C. & Van De Meerakker, S. Y. T. Imaging resonances in low-energy NO-He inelastic collisions. *Science* **350**, 787–790 (2015).
19. Onvlee, J., Gordon, S. D. S., Vogels, S. N., Auth, T., Karman, T., Nichols, B., Van Der

Avoird, A., Groenenboom, G. C., Brouard, M. & Van De Meerakker, S. Y. T. Imaging quantum stereodynamics through Fraunhofer scattering of NO radicals with rare-gas atoms. *Nat. Chem.* **9**, 226–233 (2017).

20. Klein, A., Shagam, Y., Skomorowsky, W., Zuchowski, P. S., Pawlak, M., Janssen, L. M. C., Moiseyev, N., van de Meerakker, S. Y. T., van der Avoird, A., Koch, C. P. & Narevicius, E. Directly probing anisotropy in atom-molecule collisions through quantum scattering resonances. *Nat. Phys.* **13**, 35–38 (2017).
21. Brouard, M., Parker, D. H. & van de Meerakker, S. Y. T. Taming molecular collisions using electric and magnetic fields. *Chem. Soc. Rev.* **43**, 7279–7294 (2014).
22. Balakrishnan, N., Forrey, R. C. & Dalgarno, A. Quenching of H_2 vibrations in ultracold ^{3}He and ^{4}He collisions. *Phys. Rev. Lett.* **80**, 3224–3227 (1998).
23. Sultanov, R. A. & Balakrishnan, N. Oxygen Chemistry in the Interstellar Medium: The Effect of Vibrational Excitation of H_2 in the $O(^3P)$+H_2 Reaction. *Astrophys. J.* **629**, 305–310 (2005).
24. Dos Santos, S. F., Balakrishnan, N., Lepp, S., Quéméner, G., Forrey, R. C., Hinde, R. J. & Stancil, P. C. Quantum dynamics of rovibrational transitions in H_2-H_2 collisions: Internal energy and rotational angular momentum conservation effects. *J. Chem. Phys.* **134**, 214303 (2011).
25. Nolte, J. L., Yang, B. H., Stancil, P. C., Lee, T. G., Balakrishnan, N., Forrey, R. C. & Dalgarno, A. Isotope effects in complex scattering lengths for He collisions with molecular hydrogen. *Phys. Rev. A - At. Mol. Opt. Phys.* **81**, 014701 (2010).
26. Jambrina, P. G., Croft, J. F. E., Guo, H., Brouard, M., Balakrishnan, N. & Aoiz, F. J. Stereodynamical Control of a Quantum Scattering Resonance in Cold Molecular Collisions. *Phys. Rev. Lett.* **123**, 43401 (2019).
27. Shagam, Y., Klein, A., Skomorowski, W., Yun, R., Averbukh, V., Koch, C. P. & Narevicius, E. Molecular hydrogen interacts more strongly when rotationally excited at low temperatures leading to faster reactions. *Nat. Chem.* **7**, 921–926 (2015).
28. Buck, U. Rotationally Inelastic Scattering of Hydrogen Molecules and the Non-spherical Interaction. *Faraday Discuss. Chem. Soc.* **73**, 187–203 (1982).
29. Andres, J., Buck, U., Huisken, F., Schleusener, J. & Torello, F. The anisotropic interaction potential of D_2Ne from state-to-state differential cross sections for rotational excitation. *J. Chem. Phys.* **73**, 5620–5630 (1980).
30. Faubel, M., Gianturco, F. A., Ragnetti, F., Rusin, L. Y., Sondermann, F., Tappe, U. & Toennies, J. P. The H_2-Ne interaction. *J. Chem. Phys.* **101**, 8800 (1994).
31. Toennies, J. P., Welz, W. & Wolf, G. Molecular beam scattering studies of orbiting resonances and the determination of van der Waals potentials for H-Ne, Ar, Kr, and Xe and for H_2-Ar, Kr, and Xe. *J. Chem. Phys.* **71**, 614–642 (1979).
32. Perreault, W. E., Mukherjee, N. & Zare, R. N. HD (v = 1, j = 2, m) orientation controls HD-He rotationally inelastic scattering near 1 K. *J. Chem. Phys.* **150**, 174301 (2019).
33. Zhou, H., Perreault, W. E., Mukherjee, N. & Zare, R. N. Shape resonance determined from angular distribution in D_2 (v = 2, j = 2) + He → D_2 (v = 2, j = 0) + He cold scattering. *J. Chem. Phys.* **154**, 1–6 (2021).
34. Zhou, H., Perreault, W. E., Mukherjee, N. & Zare, R. N. Quantum mechanical double slit for molecular scattering. *Science* **374**, 960–964 (2021).
35. Miller, W. B., Safron, S. A. & Herschbach, D. R. Exchange reactions of alkali atoms with alkali halides: A collision complex mechanism. *Discuss. Faraday Soc.* **44**, 108–122

(1967).
36. Perreault, W. E., Mukherjee, N. & Zare, R. N. Angular and internal state distributions of H_2^+ generated by (2+1) resonance enhanced multiphoton ionization of H_2 using time-of-flight mass spectrometry. *J. Chem. Phys.* **144**, 214201 (2016).
37. Perreault, W. E., Mukherjee, N. & Zare, R. N. Supersonic beams of mixed gases: A method for studying cold collisions. *Chem. Phys.* **514**, 150–153 (2018).
38. Saloman, E. B. & Sansonetti, C. J. Wavelengths, energy level classifications, and energy levels for the spectrum of neutral neon. *J. Phys. Chem. Ref. Data* **33**, 1113–1158 (2004).
39. Mukherjee, N., Perreault, W. E. & Zare, R. N. Stark-induced adiabatic Raman ladder for preparing highly vibrationally excited quantum states of molecular hydrogen. *J. Phys. B At. Mol. Opt. Phys.* **50**, 144005 (2017).
40. Perreault, W. E., Zhou, H., Mukherjee, N. & Zare, R. N. Coherent Preparation of Highly Vibrating and Rotating D_2 Molecules. *J. Phys. Chem. Lett.* **13**, 4682–4687 (2022).
41. Mukherjee, N., Dong, W. & Zare, R. N. Coherent superposition of M-states in a single rovibrational level of H_2 by Stark-induced adiabatic Raman passage. *J. Chem. Phys.* **140**, 074201 (2014).
42. Jambrina, P. G., Morita, M., Croft, J. F. E., Aoiz, F. J. & Balakrishnan, N. Role of Low Energy Resonances in the Stereodynamics of Cold He + D_2 Collisions. *J. Phys. Chem. Lett.* 4064–4072 (2022).
43. Arthurs, A. M. & Dalgarno, A. The theory of scattering by a rigid rotator. *Proc. R. Soc. A* **256**, 540–551 (1960).
44. McKellar, A. R. W. & Welsh, H. L. Spectra of H_2-Ne and D_2-Ne Van der Waals Complexes in the Collision-Induced Fundamental Bands of Hydrogen and Deuterium. *Can. J. Phys.* **50**, 1458–1464 (1972).

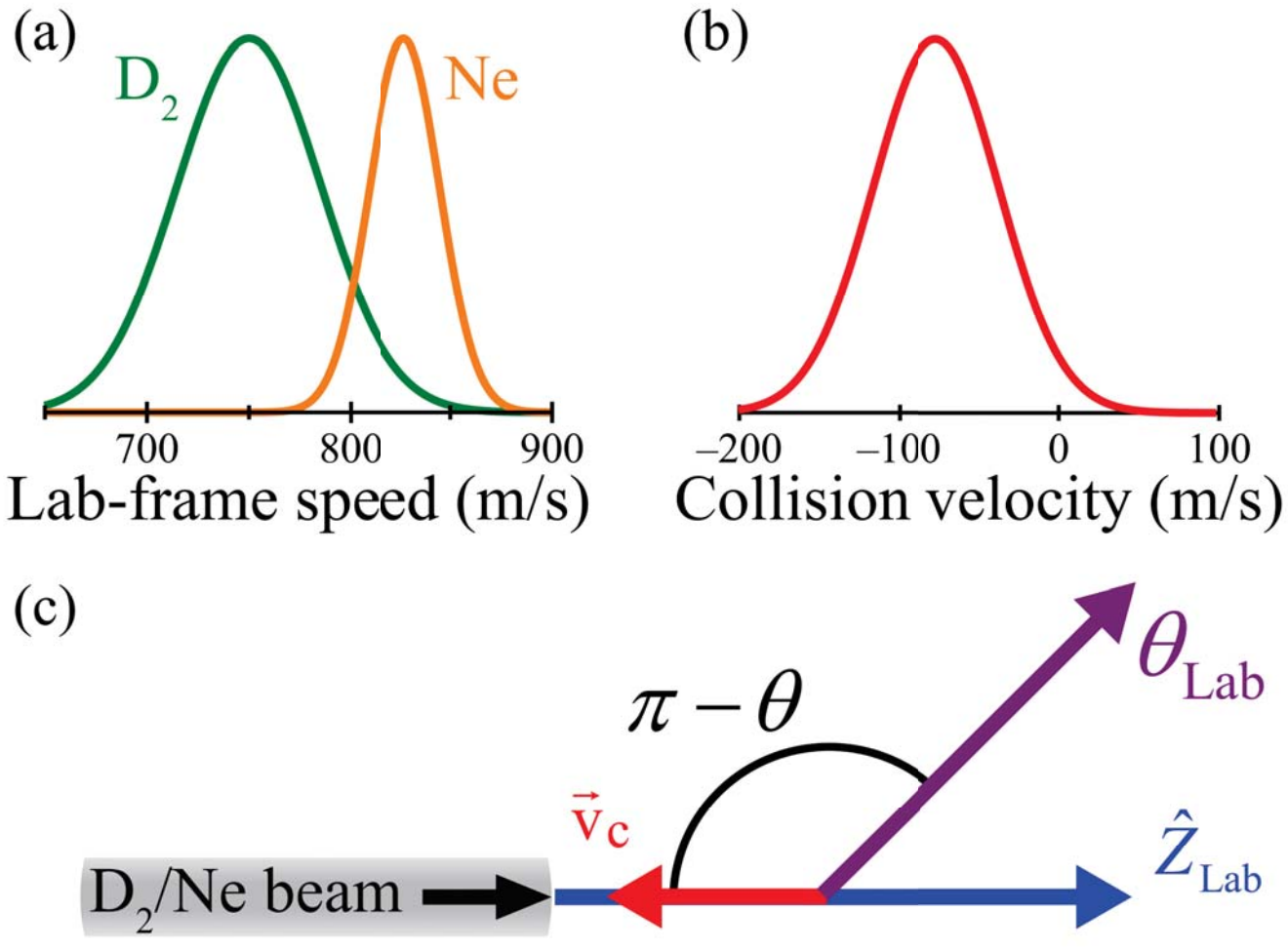
(a)
D2
Ne
700
800
900
Lab-frame speed (m/s)
(b)
–200
–100
0
100
Collision velocity (m/s)
(c)
θLab
π − θ
v⃗c
Ẑ Lab
D2/Ne beam

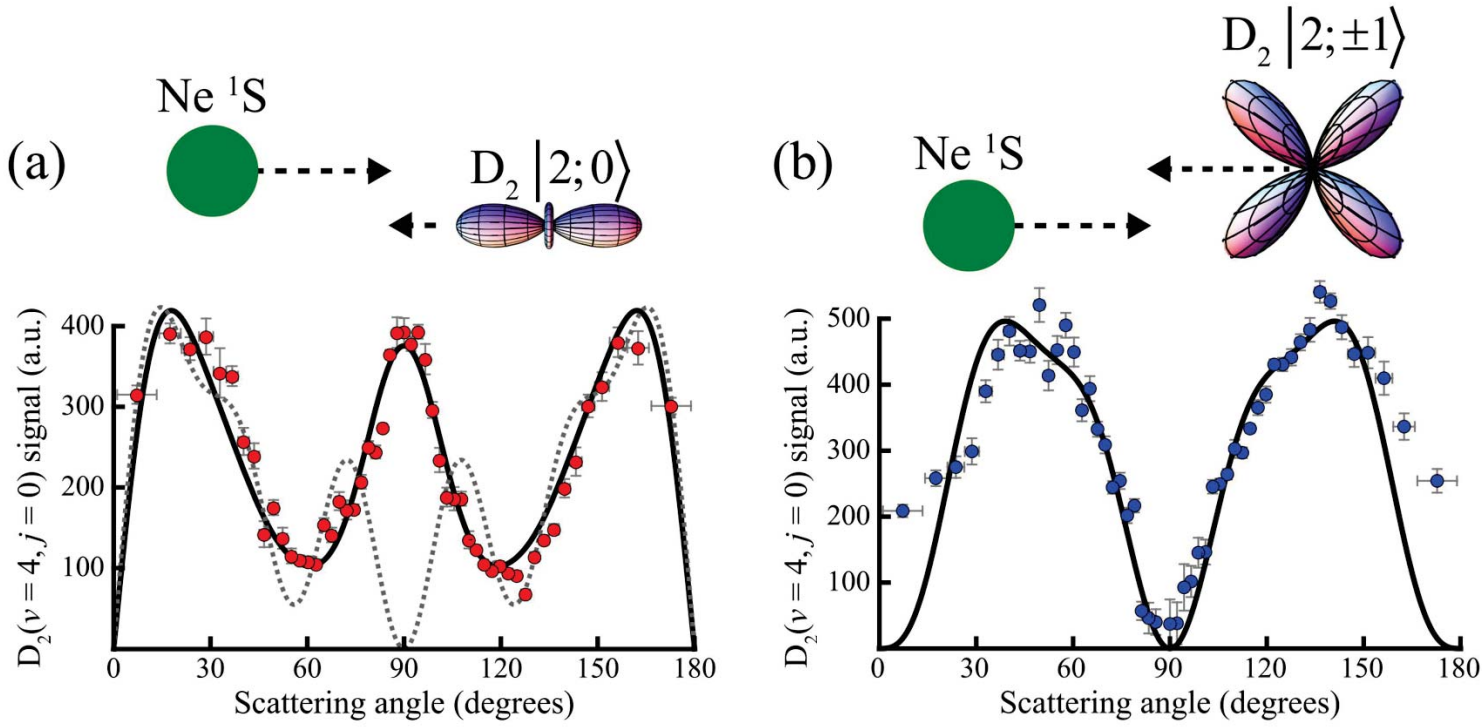
(a)
Ne ^{1}S
D$_2$ $|2;0\rangle$
D$_2$($v=4, j=0$) signal (a.u.)
Scattering angle (degrees)
(b)
Ne ^{1}S
D$_2$ $|2;\pm1\rangle$
D$_2$($v=4, j=0$) signal (a.u.)
Scattering angle (degrees)

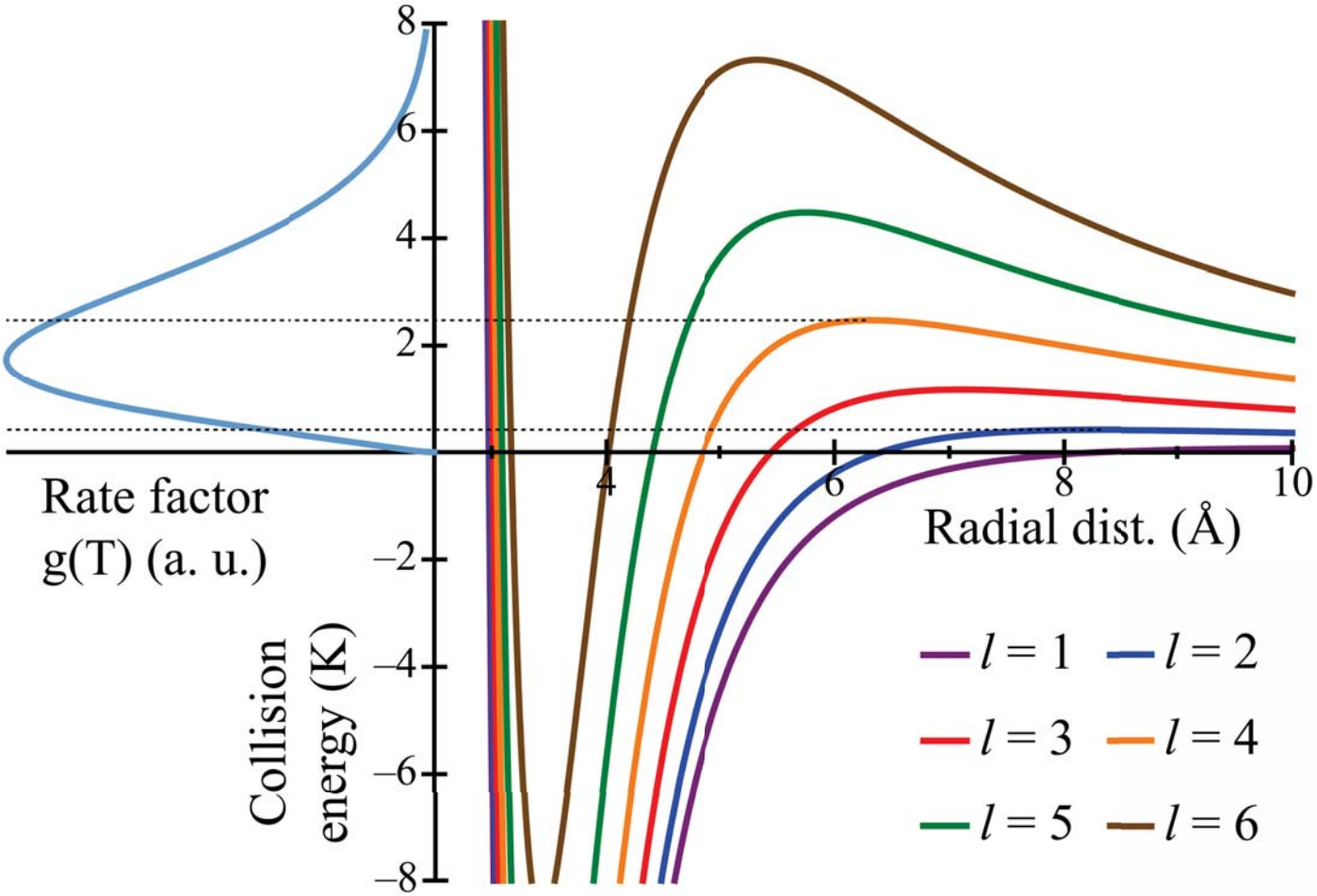
8
6
4
2
−2
−4
−6
−8
4
6
8
10
Rate factor
g(T) (a. u.)
Collision
energy (K)
Radial dist. (Å)
l = 1
l = 2
l = 3
l = 4
l = 5
l = 6